OXFORD

Lag3 and PD-1 pathways preferentially regulate NFAT-dependent TCR signalling programmes during early CD4+ T cell activation

Lozan Sheriff[1], Alastair Copland[1], David A.J. Lecky[1], Reygn Done[1], Lorna S. George[1],
Emma K. Jennings[1,2], Sophie Rouvray[1], Thomas A.E. Elliot[1,3], Elizabeth S. Jinks[1], Lalit Pallan[1],
David Bending[1,*] (iD)

[1]Department of Immunology and Immunotherapy, School of Infection, Inflammation and Immunology, College of Medicine and Health, University of Birmingham, Birmingham B15 2TT, United Kingdom
[2]Present address: Division of Biomedical Sciences, Warwick Medical School, University of Warwick, Coventry, United Kingdom
[3]Present address: Lydia Becker Institute of Immunology and Inflammation, Faculty of Biology, Medicine and Health, Manchester Academic Health Science Center, University of Manchester, Manchester, United Kingdom

*Corresponding author. Department of Immunology and Immunotherapy, School of Infection, Inflammation and Immunology, College of Medicine and Health, University of Birmingham, Birmingham B15 2TT, United Kingdom. E-mail: d.a.bending@bham.ac.uk

Abstract

Introduction:
Lag3 and PD-1 are immune checkpoints that regulate T cell responses and are current immunotherapy targets. Yet how they function to control early stages of CD4+ T cell activation remains unclear.

Methods: Here, we show that the PD-1 and Lag3 pathways exhibit layered control of the early CD4+ T cell activation process, with the effects of Lag3 more pronounced in the presence of PD-1 pathway co-blockade (CB). RNA sequencing revealed that CB drove an early NFAT-dependent transcriptional profile, including promotion of ICOS^hi T follicular helper cell differentiation.

Results: NFAT pathway inhibition abolished CB-induced upregulation of NFAT-dependent co-receptors ICOS and OX40, whilst unaffecting the NFAT-independent gene *Nr4a1*. Mechanistically, Lag3 and PD-1 pathways functioned additively to regulate the duration of T cell receptor signals during CD4+ T cell re-activation. Phenotypic changes in peripheral blood CD4+ T cells in humans on anti-Lag3 and anti-PD-1 combination therapy revealed upregulation of genes encoding ICOS and OX40 on distinct CD4+ T cell subsets, highlighting the potential translational relevance of our findings.

Conclusion: Our data therefore reveal that PD-1 and Lag3 pathways converge to additively regulate TCR signal duration and may preferentially control NFAT-dependent transcriptional activity during early CD4+ T cell re-activation.

Graphical Abstract
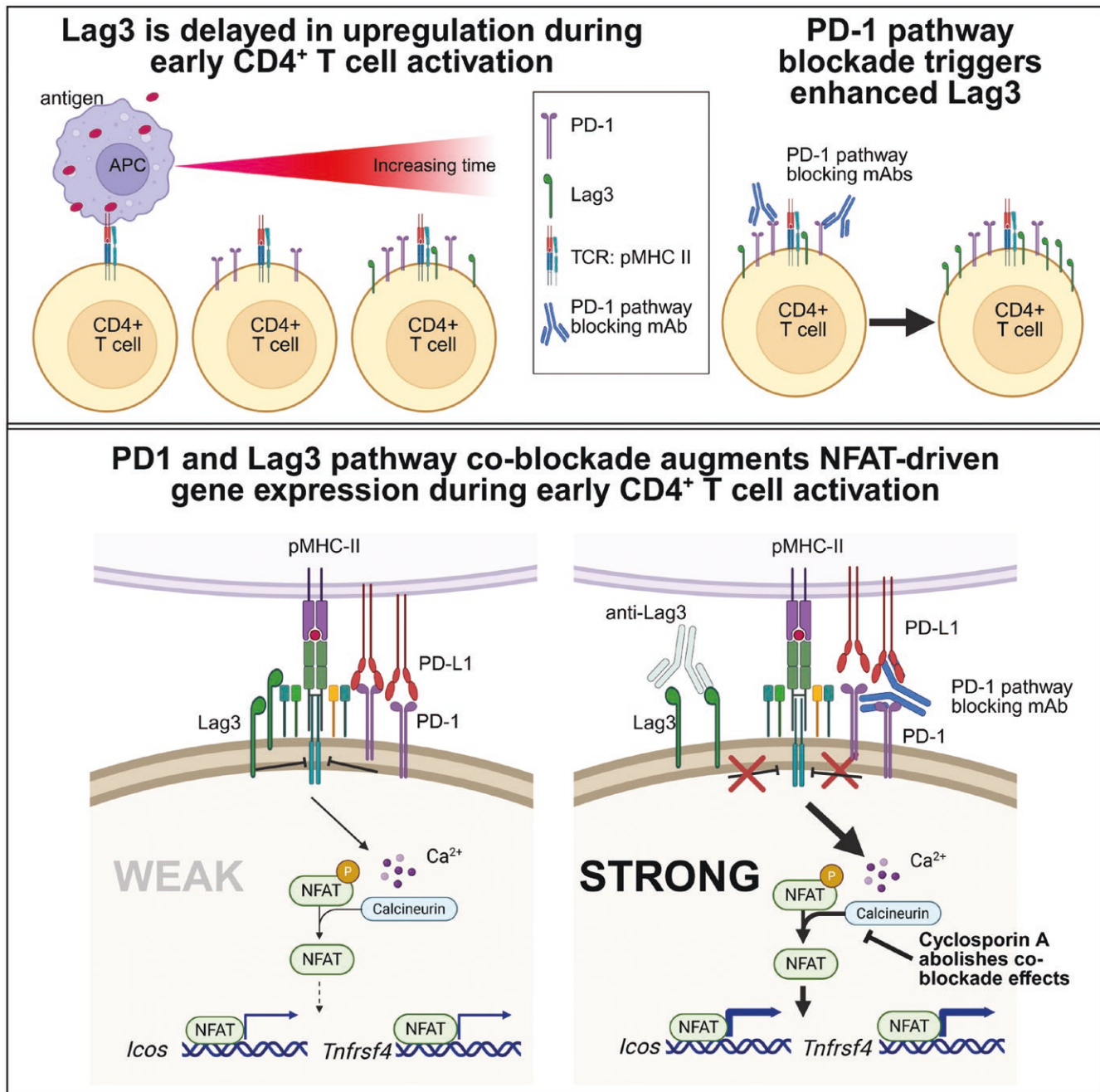
Keywords: Lag3; PD-1; TCR signaling; NFAT; CD4+ T cells; tolerance

Introduction

Canonical T cell activation is initiated by the binding of the T cell receptor (TCR) to peptide-loaded major histocompatibility complexes (MHC). The integration of signals from co-stimulatory and co-inhibitory molecules fine-tunes this process [1] and can alter the threshold for T cell activation [2]. Understanding how T cell activation thresholds are modulated has fundamental implications for the treatment of T cell-mediated diseases and the exploitation of T cell-modulating immunotherapies.

The immune checkpoints programmed cell death protein 1 (PD-1), cytotoxic T lymphocyte antigen 4 (CTLA-4) and lymphocyte activation gene 3 (Lag3), have been identified as critical regulators of T cell activation [3–5]. All three molecules (and for PD-1 also its ligand PD-L1 [6]), are current approved targets for cancer immunotherapy [7, 8]. Each of these checkpoints is thought to exhibit distinct functions on T cells. PD-1 contains immunoreceptor tyrosine-based inhibitory motifs (ITIMs) that allow it to recruit Src homology-2 domain-containing protein tyrosine phosphatase-2 (SHP-2) [9] phosphatases to target the TCR [10] and CD28 [11]. CTLA-4 acts on the CD28 pathway and competes with CD28 for binding to the costimulatory molecules CD80/ CD86 [12–14] and therefore regulates T cell co-stimulation [15]. Lag3, a CD4 structural homologue

[16], binds MHC class II [17] and is an important regulator of T cell activation and expansion [5]. Indeed, increasing evidence highlights the importance of CD4+ T cell tumour surveillance and control through recognition on peptide MHC II complexes [18]. In addition, CD4 T cells are also essential for shaping and enhancing the anti-tumour cytotoxic CD8 response [19, 20].

We recently developed an accelerated adaptive tolerance model that can evaluate the effects of immune checkpoints on CD4+ T cell activation *in vivo* [2, 21]. Using this model, we showed that PD-1 acts as a rheostat to control the threshold for T cell activation. Its blockade leads to an enhanced TCR signal strength and the upregulation of co-stimulatory molecules, such as ICOS and OX40 [2]. Importantly, we found that the co-inhibitory receptor Lag3 was strongly up-regulated in these tolerogenic CD4 T cells, and so we questioned what effect this pathway would have on T cell function in the context of PD-1 pathway blockade.

To investigate how Lag3 may regulate CD4+ T cells in the context of PD-1 pathway blockade, we exploited the Tg4 TCR transgenic model, which is specific for myelin basic protein (MBP) peptide. MBP contains a lysine (K) at position 4, which exhibits unstable MHC binding to the I-A^U class II molecule [22, 23]. Substituting for a tyrosine (Y) generates an affinity for I-A^U, which leads to highly stable peptide/MHC II complexes [22, 24], which are potently recognized by the Tg4 transgenic TCR. Given that Lag3 has a preferential function for targeting stable peptide/MHC II complexes [25, 26], we were interested to further understand its role in the context of PD-1/PD-L1 pathway blockade during longer periods of immune activation with [4Y]-MBP.

In this study, we reveal that PD-1 and Lag3 pathways exhibit layered and time-dependent control of CD4+ T cell activation. By additively regulating the duration of TCR signalling, the two pathways converge to principally regulate NFAT-dependent distal TCR signalling programmes in CD4+ T cells.

Results

PD-1 and Lag3 exhibit layered control of early CD4+ T cell re-activation

To understand the kinetic relationship between PD-1 and Lag3 expression we analysed a previous RNA-seq time course that investigated the temporal dynamics of gene expression in Tg4 T cells undergoing strong or weak TCR signalling (Fig. 1A). These data revealed that the gene encoding PD-1 (*Pdcd1*) was similarly primed by weak or strong TCR signals, behaving largely like an activation marker. In contrast, *Lag3* required higher TCR signal strengths and its peak activation was delayed compared to *Pdcd1* (Fig. 1A and B). In addition, blockade of PD-1 signalling (through anti-PD-L1) led to increased expression of Lag3 on CD4+ T cells (Fig. 1C). These data led us to hypothesize that Lag-3 and PD-1 may exert layered control of early CD4+ T cell re-activation *in vivo*.

Given the potential feedback control of Lag3 by PD-1 pathway blockade, we wanted to further understand how Lag3 and PD-1 signalling interact to control CD4+ T cell activation. To further investigate the effects of co-blockade (CB) of Lag3 and PD-L1 *in vivo*, we therefore utilized an accelerated adaptive tolerance model [2, 21] to test CB potency effects following T cell reactivation (Fig. 1D). In this model [27], a single high dose of [4Y]-MBP induces transient TCR signalling *in vivo* and upregulation of multiple immune checkpoints, including PD-1 and Lag3, thereby allowing an assessment of their functions [2]. A secondary immunization subsequently allows a dissection of the roles that Lag3 and PD-L1 play in the activation thresholds for CD4+ T cells. In this study, we employed an NFAT-dependent reporter gene *Nr4a3* [28] to study T cell activation. *Nr4a3* activates in a switch like fashion following TCR signalling [2], allowing us to identify T cells that have recently activated the NFAT pathway in vivo.

CB significantly enhanced *Nr4a3*-Red+*Nr4a3*-Blue+ (i.e. cells that have persistent activity of the NFAT-*Nr4a3* pathway [28] and henceforth referred to as "responder" cells; mean = 33.3%) compared to isotype control (mean=7.9%) and single agent anti-PD-L1 (mean = 21.7%) or anti-Lag3 (mean = 18.5%) treatment (Fig. 1E and 1F). We have previously identified ICOS and OX40 as markers of PD-1 response in CD4+ T cells [2], so we were interested to further understand their regulation in the context of CB. Analysis of ICOS and OX40 expression within responder cells (to normalize for differences in the frequency of T cell activation *in vivo*, Supplementary Fig. 1) revealed a strikingly large increase in CD4+ T cell surface expression of ICOS and OX40 in CB-recipient mice compared to IgG or single agent-treated mice (Fig. 1G, Supplementary Fig. 1). We generated a surface protein metric called surface TCR.strong based on the geometric mean of OX40 and ICOS MFI (Supplementary Fig. 2), the transcripts of which we have previously reported to be enriched in melanoma patient responders to Nivolumab [2]. Analysis of surface TCR.strong expression suggested that CB was exerting synergistic effects on the levels of OX40 and ICOS compared to individual treatments (Fig. 1H). To further explore the effects of Lag3 and PD-L1 CB on responder and surface TCR.strong metrics, we performed statistical testing to determine whether any interaction (i.e. potential synergy) existed between the treatments (Fig. 1I). The effect of CB was additive for the responder population (parallel lines, *P* value for interaction = .865, ns); however, for the surface TCR.strong metric, a significant interaction was detected, highlighting a synergistic effect on ICOS and OX40 expression. As the analysis was performed on only responder populations, this effect is not driven by differential activation states in response to the different treatment regimes. These findings were also seen at a later time point (18 h) post-secondary stimulation in independent experiments (Fig. 1J). These synergistic changes were also detected when ICOS and OX40 were analysed as separate markers (Supplementary Fig. 3). In summary, these data reveal that CB of Lag3 and PD-L1 drives additive increases in the proportion of CD4+ T cells that re-activate as well as synergistic increases in markers linked to strong TCR signalling *in vivo*.

PD-1 and Lag3 pathway blockade enhances NFAT-dependent TCR transcriptional programmes

To gain an unbiased overview of phenotypic changes in CD4+ T cells in response to CB, we repeated the experiments performed in Fig. 1D, but this time used FACS to isolate responder cell populations before performing 3′ mRNA sequencing (Fig. 2A and 2B). Isolating the responders alone (i.e. Timer+ cells) allowed us to normalize for different levels of activation between groups and to home-in on the qualitative changes
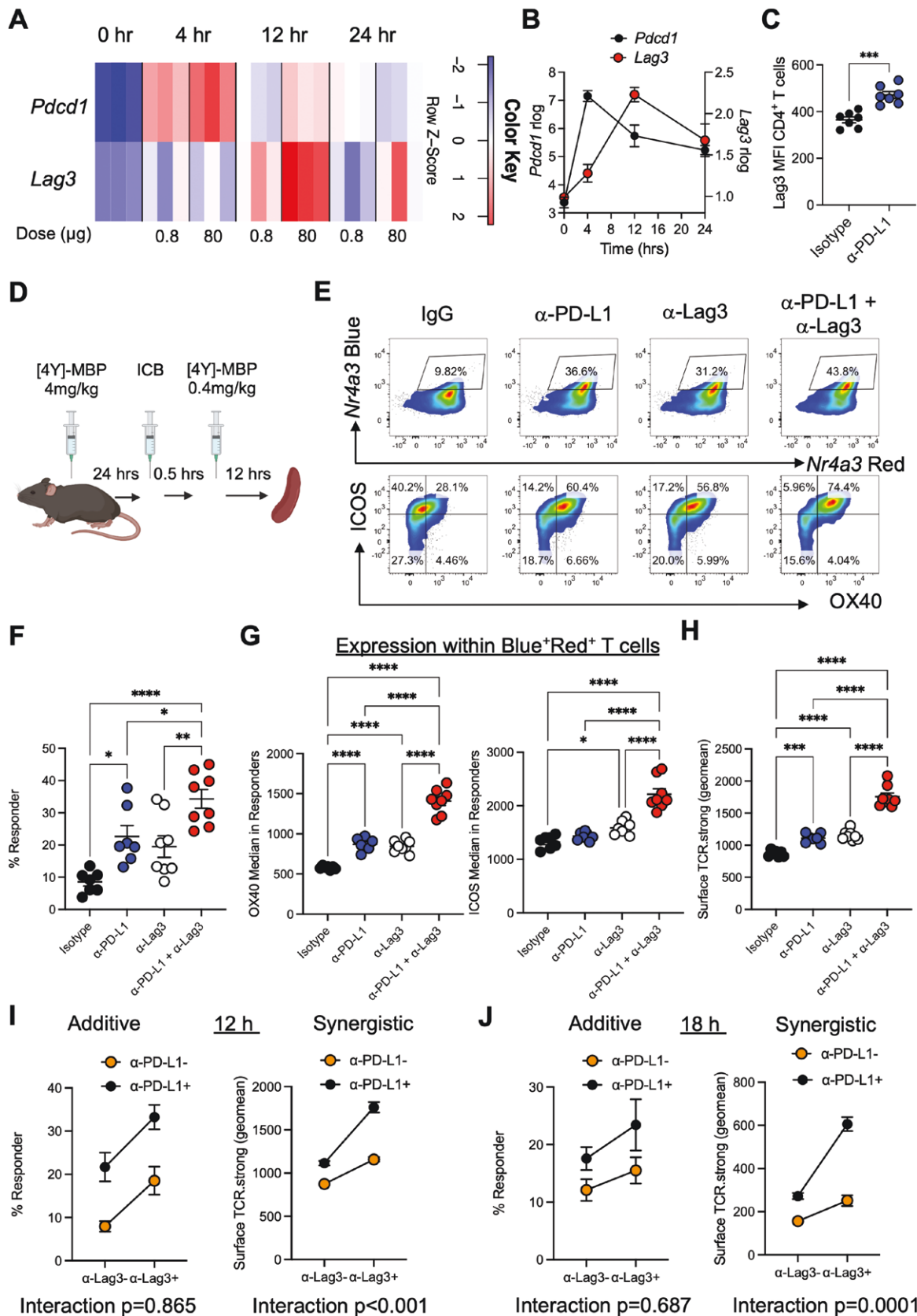
Figure 1. PD-1 and Lag3 exhibit layered control of early CD4+ T cell activation. Tg4 TCR transgenic mice were immunized with low (0.8 µg; weak) or high (80 µg; strong) amounts of antigen [4Y]-Myelin basic protein (MBP) peptide s.c. in PBS and then splenic CD4+ T cells were analysed by RNA-seq at 0, 4, 12, and 24 h post-immunization for *Pdcd1* (PD-1) and *Lag3* expression GEO: GSE165817 (**A**). (**B**) Summary of (**A**) for strongly signalled CD4+ T cells. (**C**) Tg4 *Nr4a3*-Tocky *Il10*-GFP mice were immunized s.c. with 4 mg/kg of [4Y] MBP. 24 h later mice were randomized to receive either 0.5 mg isotype or anti-PD-L1 30 min prior to re-challenge with 0.4 mg/kg [4Y] MBP peptide. Splenic CD4+ T cells were analysed for Lag3 expression 12 h after

induced by these treatments. Principal component analysis (PCA) showed that the treatments were largely separated by PC1 (main biological variation), with CB-recipient mice the most distant from isotype and anti-Lag3 and anti-PD-L1-treated mice clustering close together (Fig. 2C), with PC2 largely reflecting the batch sorting effects on the cells. Analysis of DEGs revealed that Lag3 and PD-L1 co-regulated genes associated with strong TCR signalling (*Icos, Tnfrsf4, Il21, Tnfrsf9, Maf, Irf8* [2]), but the DEG showing the highest log fold-change was the chemokine receptor *Ccr6* (Supplementary Table 1, Fig. 2D). In addition, there were notable upregulated genes involved in glycolysis/metabolism (*Aldoa, Hk2, Hif1a*), NF-kB regulator gene *Bcl3*, and genes involved in ribosome biogenesis (*Gnl3, Wdr43*). Downregulated genes included the Th2-associated *Gata3*, as well as integrins *Itga4, Itga6* and also genes involved in lymphoid tissue retention (*Sell, S1pr1*) (Fig. 2E). As we have observed previously [2] in strongly signalling CD4+ T cells, genes encoding molecules involved in TCR signalling were also downregulated (*Cd4, Rasgrp2*). Having noticed a reduction in Gata3 (Th2 master transcription factor), we curated an analysis of genes associated with different T helper subsets (Fig. 2F). Visualization revealed a clear footprint for Tfh cells (notable differences for *Il21, Icos,* and *Maf*) and Th17-associated markers (although *Il17a* and *Il17f* transcripts were not detectable), including *Ccr6*, which was also elevated in anti-PD-L1 treated mice (Fig. 2F). Th1-, Th2-, and Treg-associated transcripts were less pronounced after CB treatment, albeit with clear variation in expression, reflecting low transcript abundance for many of these genes.

Since transcriptional analysis by RNA-seq provides only a 'snapshot-in-time' view, we verified protein levels of the other notable markers identified previously. We performed an identical experiment as in Fig. 2A and then evaluated protein intracellular levels of IRF8 (a DEG and part of the TCR.strong metric [2]) and IRF4 (previously linked in this model to strong TCR signalling [2]) (Supplementary Fig. 4A and 4B). Analysis revealed that CB increased levels of IRF8 compared to all three treatment groups, whilst for IRF4 CB increased the levels compared to control and anti-PD-L1 treated mice. In addition, we validated whether the upregulation of *Ccr6* also occurred at the protein level. Analysis of surface CCR6 revealed a sharp, synergistic upregulation (more than 30% of cells now positive for this marker) in response to CB (Supplementary Fig. 4C and 4D) and that CB treated CD4+ T cells showed enhanced migration towards the chemokine CCL20 (Supplementary Fig. 4E). In addition, we confirmed that the early differentiation of ICOS^hi Tfh cells were significantly increased by CB in the Tg4 model (Supplementary Fig. 5A–D) and that in a polyclonal NP-ova immunization model, CB also consistently drove increased CD4+ICOS+ and Tfh cell differentiation, albeit with the major contribution coming from PD-1 pathway inhibition (Supplementary Fig. 5E–H).

Given that *Nr4a3* is a direct NFAT target [28] and that Tfh cells are known to develop under AP-1 independent NFAT signalling [30], we wanted to further understand whether the DEGs identified showed any relationship to NFAT signalling pathways. A recent study determined that 1089 genes in T cells are directly regulated by NFAT and ERK pathways during the first 30 h [29]—a similar time frame to our *in vivo* studies. Through incorporation of inhibitors of NFAT or ERK pathways, Wither *et al.* determined the relative dependence of genes on these signalling axes. We intersected the 189 genes that were upregulated in CD4+ T cell responders between CB-treated and isotype-treated mice with the 309 identified in Wither *et al.* as showing largely NFAT-dependence. Thirty-nine genes were found to overlap between the two data sets (Fig. 2G). We performed gene set enrichment analysis (GSEA) based on the annotation of Wither *et al.* [29] for largely NFAT-dependent (Fig. 2H) or largely ERK-driven pathway dependent genes (Fig. 2I). GSEA revealed significant enrichment for largely NFAT-dependent genes (Fig. 2H, NES = 2.73, FDR = 0.000) but no enrichment for the predominantly ERK-driven target genes (Fig. 2I, NES = 0.92, FDR = 0.664). Visualization of the predominantly NFAT-dependent genes across the four conditions showed that only CB-treated CD4+ T cells clustered as a discrete group, and hallmark genes such as *Irf8, Tnfrsf4, Icos, Irf4, Il2ra, Lag3* and *Pdcd1* were all part of the core enrichment set (Fig. 2J). Taken together, CB imparts a novel transcriptional signature on CD4+ T cells undergoing reactivation *in vivo*, exhibiting hallmarks of NFAT-biased TCR signalling and early promotion of Tfh cell differentiation.

NFAT pathway inhibition abolishes the major effects of PD-1 and Lag3 pathway co-blockade

Given the significant enrichment of gene and transcriptional programmes that show a large NFAT dependence, we wanted to functionally explore this pathway. We established a new *in vitro* model to assess the relative contributions of the PD-L1 and Lag3 pathways controlling *in vitro* TCR signal strength in adaptively tolerized T cells (Fig. 3A). Splenocytes from Tg4 *Nr4a3*-Tocky *Il10*-GFP mice were isolated 24 h after *in vivo* immunization and cultured in the presence of isotype control or CB in the presence of a dose titration of [4Y]-MBP (Fig. 3A to 3C). To demonstrate that this model can reveal manipulations into TCR signalling, we evaluated OX40 and ICOS expression on CD4+ T cells. Both OX40 (Fig. 3B) and ICOS expression (Fig. 3C) were upregulated by CB across a range of agonist peptide concentrations.

We then determined the sensitivity of OX40 (predominantly NFAT, strong) and ICOS (predominant NFAT, weak) to NFAT-pathway inhibition (Fig. 3D to 3G). We also included Nur77, which we have shown to be NFAT-pathway

peptide re-challenge. (**D**) Experimental setup and interpretation for part (**E**). Tg4 *Nr4a3*-Tocky *Il10*-GFP mice were immunized s.c. with 4 mg/kg of [4Y] MBP. Twenty-four hours later, mice were randomized to receive either 0.5 mg isotype pool (1:1 ratio of rat IgG1 and rat IgG2a), anti-Lag3, or anti-PD-L1 or a combination of both 30 min prior to re-challenge with 0.4 mg/kg [4Y] MBP peptide. Splenic CD4+ T cells were analysed for *Nr4a3*-Blue versus *Nr4a3*-Red analysis at 12 h after peptide re-challenge. Flow plots showing expression of OX40 and ICOS within CD4+ T cells. (**F**) Summary data from (B) detailing percentage of responders after 12 h re-challenge. (**G**) and Summary data from (B) detailing MFI (median fluorescence intensity) of OX40 and ICOS within responding CD4+ T cells after 12 h re-challenge. (**H**) Summary data detailing geometric mean of ICOS and OX40 (surface TCR.strong) after 12 h re-challenge. (**F**)-(**H**) Isotype (*n* = 7), anti-Lag3 (*n* = 7), or anti-PD1 (*n* =8) or combination therapy (*n* = 8). Bars represent mean ± SEM, dots represent individual mice. Statistical analysis by one-way ANOVA with Tukey's multiple comparisons test. Two-way anova to test the interaction effects of percentage responders and geometric mean of surface TCR.strong between αLag3 and αPD-L1 at (**I**) 12 h (IgG *n* = 7, anti-PD-L1 = 7, anti-Lag3 = 8, and combination *n* = 8) or 18 h (**J**) post re-challenge (IgG *n* = 4, anti-PD-L1 = 5, anti-Lag3 = 5, and combination *n* = 5).
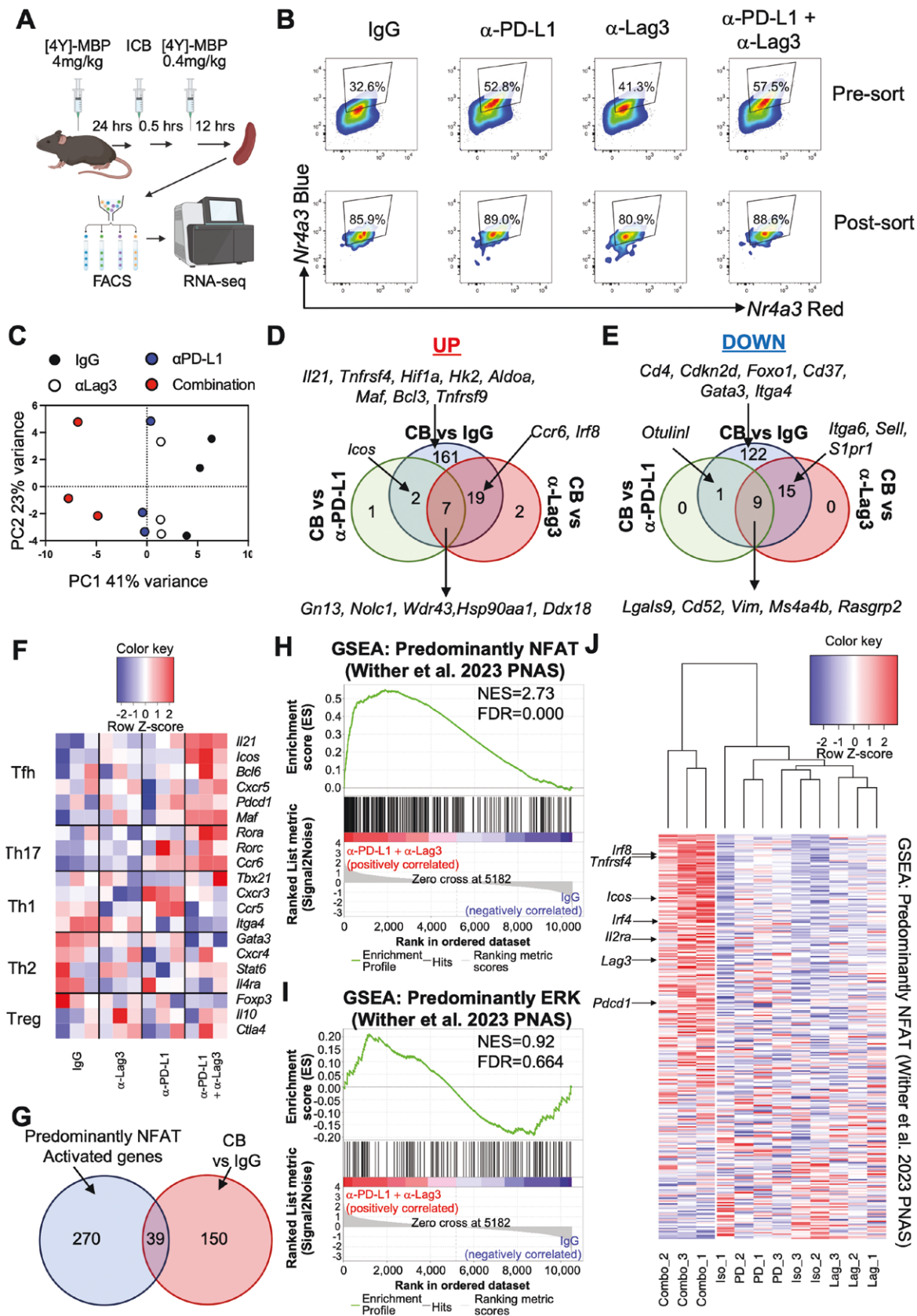
Figure 2. PD-1 and Lag3 blockade enhances NFAT-dependent TCR transcriptional programmes. (**A**) Experimental setup and interpretation for part (B). (**B**) Tg4 *Nr4a3*-Tocky *Il10*-GFP mice were immunized s.c. with 4 mg/kg of [4Y]-MBP. Twenty-four hours later mice were randomized to receive either 0.5 mg isotype pool (*n* = 3) (1:1 ratio of rat IgG1 and rat IgG2a), anti-Lag3 (*n* = 3), or anti-PD-L1 (*n* = 3) or combination therapy (*n* = 3) 30 min prior to re-challenge with 0.4 mg/kg [4Y]-MBP peptide. Twelve hours later, splenic CD4+ T cell responses were analysed for *Nr4a3*-Timer Red versus *Nr4a3*-Timer Blue expression in live CD4+Tg4 T cells and sorted for CD4+Nr4a3-Blue+Nr4a3-Red+ T cells by FACS. (**B**) Flow plots showing *Nr4a3*-Timer Blue+, *Nr4a3*-Timer

independent [28]. Nur77 expression was unaffected by CB and the frequency of Nur77-Blue$^+$ cells was also unchanged by a range of cyclosporin A (CsA) (Fig. 3D). In contrast, CB induced upregulation of OX40 showed enhanced sensitivity to CsA, and at 0.01 μM the increase in OX40 by CB was lost (Fig. 3E). CB-induced ICOS upregulation showed a similar pattern to OX40, with the effect of CB lost by 0.1 μM concentration (Fig. 3F). Summarising the percentage change revealed that the 3 markers showed alterations in expression by CB which would have been predicted based on the Wither *et al.* [29] model (Fig. 3G).

PD-L1 and Lag3 co-operatively regulate TCR signal duration in CD4$^+$ T cells

The maturation of Timer Blue proteins into Timer Red can give an estimation of the signal duration within an actively signalling T cell population (Fig. 4A). This is because TCR signalling triggers new formation of Timer Blue proteins, which have a half-life of 4 h, before maturation into the longer lived Red proteins from (half-life of 3–5 days). A short TCR signal will thus lead to an increase and then fall in Red proteins, whilst sustained signalling will lead to accumulation of mature Timer Red proteins. We hypothesized that the enhanced NFAT-biased signature observed is a result of CB sustaining TCR signalling for a longer period following re-activation *in vivo* and we therefore re-analysed the levels of Timer Red protein within "responder" cells from Fig. 1I and 1J across the four treatment groups. Analysis at 12 h post-reactivation in the presence of CB showed a small but significant accumulation of Timer Red proteins compared to the three other groups; however, a small increase in Timer Red was also observed in the anti-PD-L1-treated mice (Fig. 4B). Analysis at the later 18 h timepoint revealed that only CB exhibited a significant increase in Timer Red, which demonstrates that these cells have signalled for a longer period (Fig. 4C).

We next wanted to test whether key NFAT-dependent markers identified in Fig. 2 were regulated by the duration of TCR signalling. We cultured antigen-adapted Tg4 T cells *in vitro* in the presence of [4Y]-MBP and added the Src kinase inhibitor PP2 to terminate TCR signalling after 0, 4, 8, 12, or 24 h (Fig. 4D). Cells remained in culture for the full 24 h before analysis of Nr4a3-Blue, ICOS, OX40, and IRF8 expression. As expected, *Nr4a3*-Blue expression continued to increase in parallel with the increase in TCR signal duration (Fig. 4E). ICOS expression showed a delayed response but rose prominently from 4 h to 12 h with a gradual increase up to 24 h (Fig. 4E). IRF8 showed a similar pattern but its induction required longer periods of TCR signalling (minimum of 12 h), and gradually increased thereafter (Fig. 4E). OX40 showed a time dependent increase from the initiation of TCR signalling but plateaued from 12 to 24 h (Fig. 4E). Thus, CB results in an increased duration of TCR signalling, which accounts for the time-dependent and synergistic upregulation of NFAT-dependent markers ICOS, IRF8 and OX40.

Phenotypic changes in human peripheral blood CD4$^+$ T cells mirror murine changes in response to PD-1 and Lag3 immunotherapy

A recent study provided insight into transcriptional changes occurring on therapy in peripheral blood T cells in patients receiving anti-PD-1 and anti-Lag3 combination therapy (specifically Relatlimab and Nivolumab [31]). We investigated whether transcriptional changes identified in our murine models were also reflected in this cohort of human patients on combination therapy. We selected DEGs in human CD4 naive/central memory (CM), human CD4 effector memory (EM)/Th1 and human Treg and intersected these with DEGs identified between combination therapy treated murine CD4s and controls (Fig. 5A–C). Upregulated across all four conditions was the NF-kB regulator gene *BCL3/Bcl3*, which has also been linked to inhibiting Treg development and function [32]. Interestingly, *ICOS* showed upregulation across human CD4 naïve/CM and EM/Th1 cells. In addition, *CCR6* was upregulated within human effector memory/Th1 subsets.

In human Treg, the gene encoding OX40 (*TNFRSF4*) was also notably upregulated, along with *PDCD1, LAG3 (*both largely NFAT-dependent), *TENT5C* (mRNA stabilization and NFAT driven). Notable downregulated genes in all four subsets included *GATA3* (Th2) and *TRAF3IP3* (required for Treg maintenance and function [33]). Human CD4 effector memory cells also showed downregulation of *DGKA* and *SIT1* (involved in TCR signalling). Notable other genes downregulated in human CD4 T EM/Th1 group also included *CORO1A, CDC25B* (cell cycle regulation) and *ANXA6* (involved in IL-2 sensing [34]) and *RAC2* (deficiency of which affects T cell activation [35]), and *ITGA4* (linked in mice to Th1 cell homing [36]). These findings confirm that peripheral human CD4$^+$ T cells reflect key marker changes observed in murine CD4$^+$ T cells, identifying ICOS, OX40, and CCR6 as potential candidates for treatment monitoring.

Discussion

Our study demonstrates that the PD-1 and Lag3 pathways exert non-redundant control on the duration of TCR signalling during early CD4$^+$ T cell re-activation. PD-1 itself can directly target the TCR [10] and CD28 [11] molecules, which allows PD-1 to act as a rheostat to control TCR signal strength [2]. PD-1 contains tyrosine-based motifs (ITIM and ITSM [37]) that allow recruitment of SHP-2 phosphatases that mediate its inhibitory function [9]. Lag3 on the other hand has proven more enigmatic in its function. Whilst its binding to MHC Class II is well established [25, 26], Lag3 also has other reported ligands of relevance to T cell biology: galectin-3 [38],

---

Red$^+$ pre and post sorting. (**C**) RNA was extracted from the sorted populations and 3′ mRNA sequencing performed. PCA of the normalized expression data identifies four clusters. Venn diagram analysis of up (**D**) or down (**E**) regulated DEGs in mice receiving combination therapy compared to the three other experimental conditions. (**F**) Z score heatmap analysis of rLog expression of genes involved in CD4$^+$ T helper subsets from Isotype (IgG), anti-Lag3, anti-PD-L1, or CB treated mice. (**G**) Intersection of the 189 genes that were upregulated in CD4$^+$ T cell responders between CB-treated and Isotype-treated mice with the 309 identified in Wither *et al.* [29] as predominantly NFAT dependent. Gene set enrichment analysis (GSEA) of NFAT- (**H**) or ERK- (**I**) dependent signalling based on classification from Wither *et al.* [29]. (**J**) Heatmap visualization of the normalized counts of the 283/309 genes with largely NFAT-dependent activity visualized across the four treatment conditions and scaled by row values and clustered by columns.
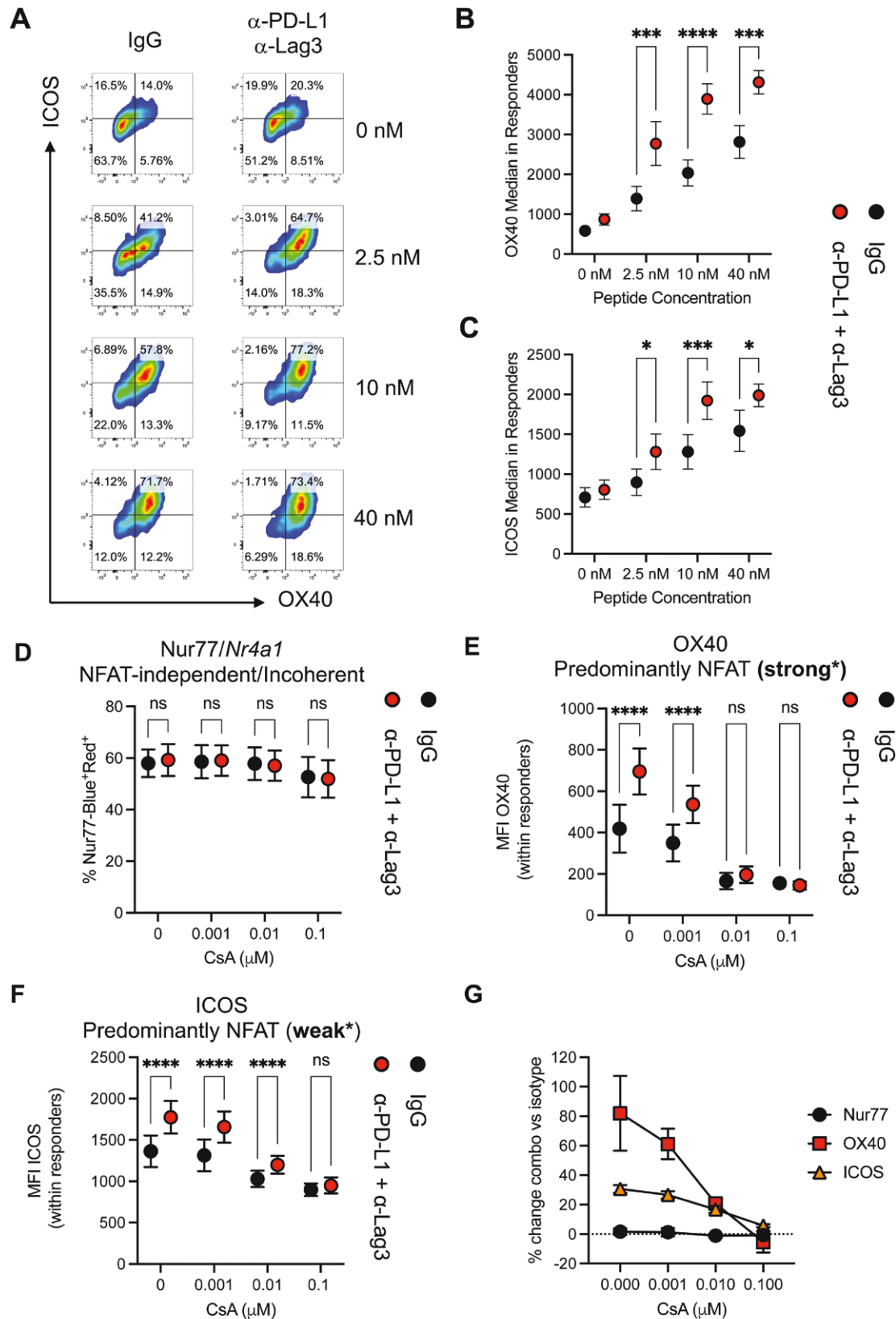
Figure 3. NFAT pathway inhibition abolishes the major effects of PD-1 and Lag3 pathway co-blockade. (**A**) Tg4 *Nr4a3*-Tocky *Il10*-GFP mice were immunized s.c. with 4 mg/kg of [4Y]-MBP peptide. Twenty-four hours post immunization splenocytes were cultured for another 24 h and rechallenged with 0, 2.5, 10, and 40 nM [4Y]-MBP peptide in presence of isotype pool or a combination of αPD-L1 and αLag-3. Splenic CD4⁺ T cell responses were analysed for OX40 and ICOS within the responding T cells after 24 h culture. Summary data from (**A**) detailing MFI (median fluorescence intensity) of OX40 (**B**) and ICOS (**C**) within responding CD4⁺ T cells after 24 h culture, (*n* = 7, pooled from two independent experiments). (**D-G**) Tg4 Nur77-Tempo

fibrinogen-like protein 1 (FLP-1) [39] and the TCR-CD3 complex [40]. Whilst stable peptide MHC Class II appear more important than FLP-1 for T cell inhibition *in vitro*, the hierarchy of ligands *in vivo* remains unclear [41]. Our findings show that Lag3 works co-operatively with the PD-1/PD-L1 pathway to regulate the T cell activation threshold of CD4⁺ T cells *in vivo*. Mechanistically, co-blockade of PD-L1 and Lag3 results in an increased duration of TCR signalling, which drove synergistic increases in NFAT-dependent pathways.

Interestingly, the effect of Lag3 blockade alone was generally weaker than the PD-L1 pathway *in vivo*, which Vignali and colleagues have also previously noted [40]. In addition, Lag3 had minor effects on the primary CD4⁺ T cell response and its major effects were only exerted in the presence of PD-1 pathway blockade. These findings may be due to broader T cell PD-1 expression and the susceptibility of Lag3 to ADAM-mediated shedding [42]. Indeed, ADAM-resistant forms of Lag3 confer resistance to anti-PD-1 immunotherapy *in vivo* [43], which is linked to reduced CD4⁺ T cell help for CD8⁺ T cells. It is possible that PD-1 blockade itself may augment the ability of Lag3 to interact with its potential ligands (e.g. MHC class II), which could result in an increased potency of Lag3 in our model, particularly as [4Y]-MBP peptide generates highly stable peptide-MHC II complexes. Given that in the immunized setting blockade of Lag3 resulted in much weaker effects than in the adaptive tolerance conditions, this may reflect the higher levels of Lag3 that are induced on the tolerised CD4⁺ Tg4 T cells.

The fact that PD-1 pathway appears more potent than Lag3 likely also reflects hierarchical levels of T cell tolerance, whereby upon loss of the PD-1 pathway, Lag3 plays a much greater functional role. It is also likely that blockade of the PD-1 pathway may alter the dwell times of T cells on APCs *in vivo*. Tolerised islet antigen-specific T cells showed enhanced motility when scanning DCs in pancreatic draining lymph node [44]. Blockade of PD-L1 or PD-1 led to reduced T cell motility and precipitation of autoimmune diabetes; however blockade of CTLA-4 had no effect on T cell motility [44] despite past reports that CTLA-4 may limit formation of stable APC:T cell conjugates [45].

A previous study demonstrated functional synergy of PD-1 and Lag3 in the control of anti-tumour immunity [46], and this was linked to increases in IFN-gamma-expressing cells amongst both CD4⁺ and CD8⁺ T cells [46]. Furthermore, several very recent studies have elegantly shown that PD-1 and Lag3 may synergise to promote CD8⁺ T cell exhaustion and hinder their cytotoxicity [47–49]. Unlike CD8⁺ T cells, CD4⁺ T cells have less clearly defined roles in tumour development, exerting anti-tumour effects through effector cytokines, cytotoxicity, and T cell help (reviewed in [50]). However, evidence for pro-tumour development comes from the association of CD4⁺ Foxp3⁺ Tregs with poor clinical outcomes [51]. Nonetheless, expansion of Tfh cells in human tumours has been observed following anti-PD-1 immunotherapy [52]. In solid tumours, Tfh cells likely have a beneficial role [53] and their tumour infiltration is positively correlated with clinical

outcome in human breast cancer [54]. Mechanistically, Tfh cell-derived IL-21 was linked to enhancing CD8⁺ T cell function in mouse models of lung adenocarcinoma [55]. Our study also suggests that CB may drive enhanced TCR signal duration and/ or signal strength. TCR signal strength has been linked to the development of T cell dysfunction and cancer development [56], so it will be important to study the impact of CB on TCR signal avidity during CD8⁺ T cell responses in cancer.

Although this study does did not seek to evaluate the impact of the tumour microenvironment on checkpoint blockade, it has highlighted that re-activation of CD4⁺ T cell under anergising conditions in the presence of CB (i.e. lack of co-stimulation) results in the emergence of NFAT-dependent TCR signalling programmes. In addition, a study assessing cancer-irrelevant immune responses to seasonal flu vaccination describe an increased Tfh cell response in patients on anti-PD-1 therapy [57]. Tfh cell signatures are also positively correlated with immune related adverse events (irAEs) in humans [58]. Interestingly, similar findings have been observed in murine studies using aged mice (18–24 months), which showed the development of IgG-mediated disease that was linked to an IL-21-producing Tfh-like subset [59]. In the present study, combination treatment robustly drove enhanced Tfh cell development, but its most notable effect was the induction of elevated NFAT-pathway dependent molecules such as OX40 and ICOS expression. Given that ICOS is an essential costimulatory molecule for Tfh cell responses *in vivo* [60], it will be important to understand its wider potential effects on humoral immunity.

The potential manipulation of Tfh cell biology by checkpoint blockade may come with inherent risk. Genetic analysis of SNPs have linked a variant (rs17388568) associated with increased risk of ulcerative colitis [61] and type 1 diabetes [62] with an enhanced response to anti-PD-1 in metastatic melanoma patients [63]. The risk variant maps to a genomic region containing *IL2* and *IL21*, which are critical cytokines involved in regulation of CD4⁺ and Tfh cell responses. Future work should address the extent to which Tfh cell development is altered in patients on immune therapies targeting PD-1 and/ or Lag3 pathways and how these relate to irAEs.

In summary, our study provides new insight into how the PD-1 and Lag3 pathways intersect to govern the duration of TCR signalling during CD4⁺ T cell activation. The co-blockade of these receptors can preferentially enhance early NFAT-dependent TCR signalling programmes and the differentiation of Tfh cells.

Materials and methods

Mice

Nr4a3-Tocky [64] lines were modified by mating to Tg4 *Il10*-GFP mice as previously described [65] to generate Tg4 *Nr4a3*-Tocky *Il10*-GFP mice [28] (unmodified Nr4a3-Tocky lines were originally obtained from Dr Masahiro

---

Il10-GFP mice were immunized s.c. with 4 mg/kg of [4Y]-MBP peptide. Twenty-four hours post immunization splenocytes were cultured for another 24 h and stimulated with 2.5 nM [4Y]-MBP peptide in presence of isotype or a combination of αPD-L1 and αLag-3 and a dose range of cyclosporin A (CsA). After 24 h the frequency of CD4⁺Nur77-Blue⁺Red⁺ T cells (**D**), median expression of OX40 (**E**), or median expression of ICOS (**F**) in CD4⁺Nur77-Blue⁺Red⁺ T cells was evaluated. (**G**) The percentage change between isotype and combination therapy was calculated for the markers for each dose of CsA. Black circles (isotype treated, *n* = 4) and red circles (combination-treated, *n* = 4, representative of two independent experiments) culture conditions. Bars represent mean ± SEM. Statistical analysis by two-way repeated-measures ANOVA with Tukey's multiple comparisons test.
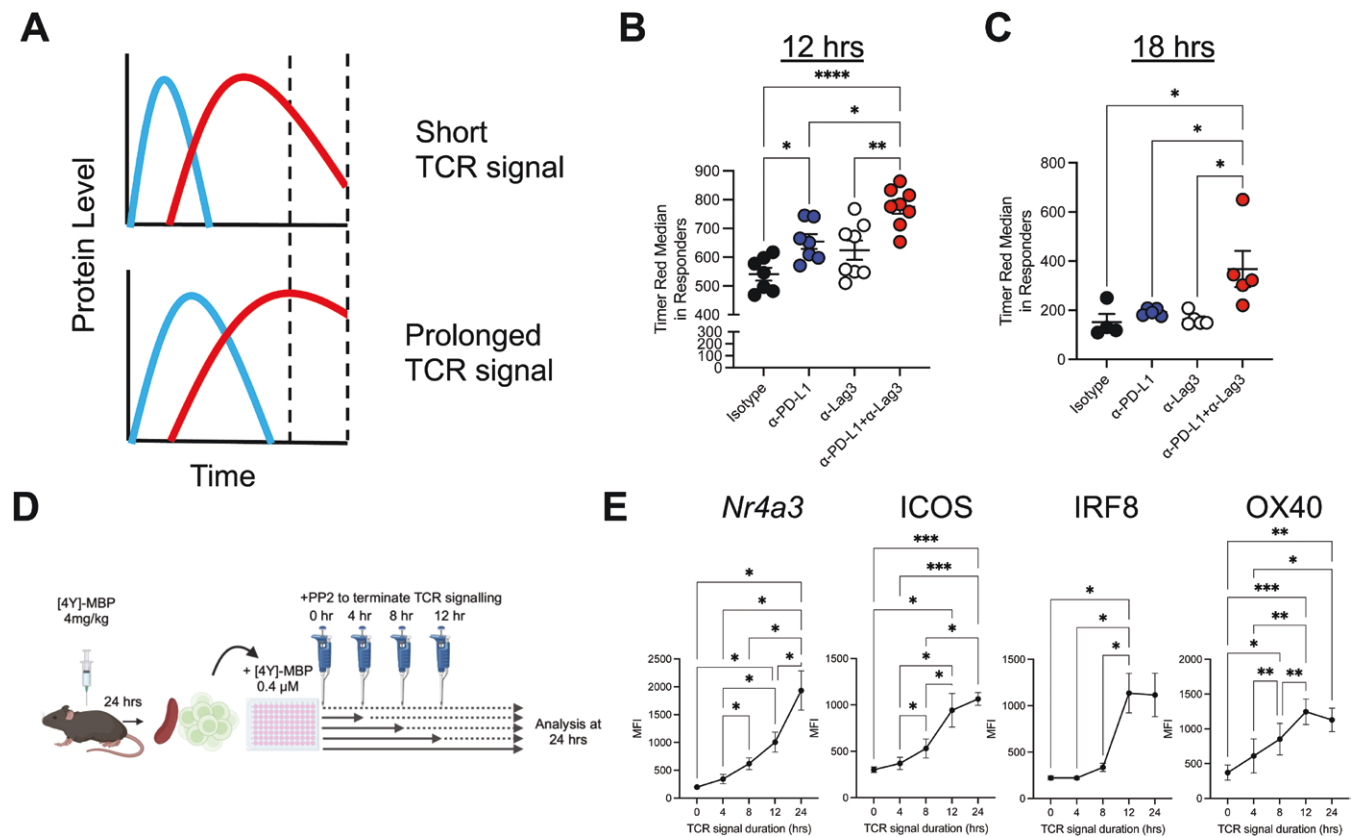
Figure 4. PD-L1 and Lag3 co-operatively regulate TCR signal duration in CD4⁺ T cells. (**A**) Graphical illustration of the levels of *Nr4a3*-Blue and *Nr4a3*-Red following a short or prolonged TCR signal. Tg4 *Nr4a3*-Tocky *Il10*-GFP mice were immunized s.c. with 4 mg/kg of [4Y]-MBP. Twenty-four hours later, mice were randomized to receive either 0.5 mg isotype pool (1:1 ratio of rat IgG1 and rat IgG2a), anti-Lag3, or anti-PD-L1 or CB 30 min prior to re-challenge with 0.4 mg/kg [4Y] MBP peptide. Twelve hours and 18 h later mice were culled and splenic responses were analysed for *Nr4a3*-Timer Red expression in responder populations. (**B**) Summary of data at 12 h post re-challenge showing red median within responders. Isotype (*n* = 7), anti-Lag3 (*n* = 7), or anti-PD-L1 (*n* = 8) or combination (*n* = 8). Bars represent mean ± SEM, dots represent individual mice. Statistical analysis by one-way ANOVA with Tukey's multiple comparisons test. (**C**) Summary of data at 18 h post re-challenge showing Timer Red median within responders. Isotype (*n* = 4), anti-Lag3 (*n* = 5), or anti-PD-L1 (*n* = 5) or combination (*n* = 5). Bars represent mean ± SEM, dots represent individual mice. (**D**) Experimental setup and interpretation for part (E). Mice were immunized s.c. with 4 mg/kg of [4Y]-MBP. Twenty-four hours later, mice were euthanized, and spleens were harvested. Splenocytes were cultured with 0.1 μM [4Y]-MBP for another 24 h and 10 μM PP2 was added to terminate TCR signalling at different time points (0 h, 4 h, 8 h, and 12 h and 24 h) before analysis by flow cytometry. (**E**) Summary data showing MFI (median fluorescence intensity) of *Nr4a3*-Timer Blue, ICOS, OX40, or IRF8 in response to different duration of TCR signalling. (*n* = 6 *Nr4a3*-Blue, ICOS, OX40); *n* = 5, IRF8). Statistical analysis by one-way ANOVA with Tukey's multiple comparisons test.

Ono (Imperial College London) under MTA; the manuscript does not report any findings arising from the use of unmodified *Nr4a3*-Tocky lines or modified *Nr4a3*-Tocky lines that have not been previously reported in the literature. Nur77-Tempo mice [66] were mated to Tg4 *Il10*-GFP mice to generate Tg4 Nur77-Tempo mice. C57BL/6J mice were purchased from Charles River. All animal experiments were approved by the local animal welfare and ethical review body and authorized under the authority of Home Office licenses P18A892E0A and PP9984349 (held by D.B.). Animals were housed in specific pathogen-free conditions. Both male and female mice typically aged 6–8 weeks were used, and littermates of the same sex were randomly assigned to experimental groups.

Accelerated adaptive tolerance models and immunotherapy

Tg4 Nur77-Tempo *Il10*-GFP or Tg4 *Nr4a3*-Tocky *Il10*-GFP mice were immunized through subcutaneous injection of 4 mg/kg [4Y] MBP peptide PBS into the flank. For *in vivo* blockade experiments, antibodies were administrated via the

intraperitoneal (i.p.) route with 0.5 mg of anti-PD-L1 antibody (clone MIH5 [67]) or rat IgG2a (clone MAC219, kind gift from Professor Anne Cooke, University of Cambridge), *in vivo* grade anti-Lag3 (clone C9B7W BioLegend) or rat IgG1 (clone MAC221). For combination therapy experiments, anti-PD-L1 and anti-Lag3 or their corresponding isotype were pooled at 1:1 ratios. For re-challenge experiments, 30 min after immunotherapy administration a second dose of 0.4 mg/kg [4Y]-MBP peptide in PBS was administered subcutaneously to the contralateral flank. Mice were then euthanized at the indicated time points, and spleens removed to analyse systemic T cell responses.

Spleen processing and flow cytometry

Splenocytes were dissociated using scissors in 1.2 ml of digestion media containing 1 mg/ml collagenase D (Merck Life Sciences) and 0.1 mg/ml DNase I (Merck Life Sciences) in 1% FBS (v/v) RPMI for 25 min at 37°C in a thermo-shaker. Digested tissue was passed through a 70 μM filter (Greiner) and centrifuged at 1500 rpm for 5 min. Red blood cells were lysed in RBC lysis buffer (Invitrogen) for 2 min on ice before washing in 2% FBS RPMI. Resulting sample was resuspended
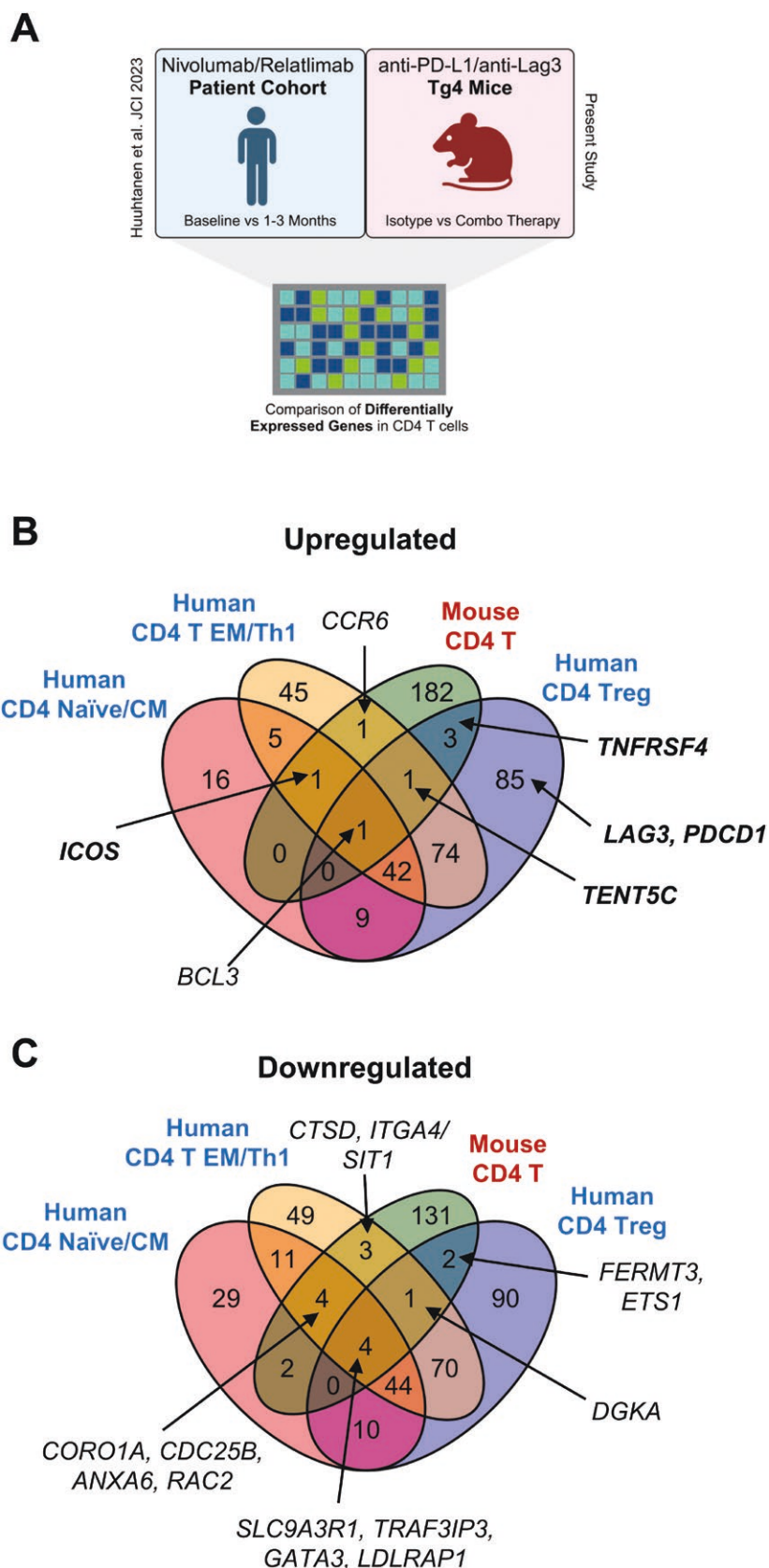
Figure 5. Phenotypic changes in human peripheral blood CD4+ T cells mirror murine changes in response to PD-1 and Lag3 immunotherapy. (**A**) Differentially expressed genes compared to month 3 or month 1 compared to baseline in CD4 Naïve or central memory, CD4 effector memory, and CD4 Treg clusters from human patients on anti-PD-1 and anti-Lag3 therapy were extracted from supplementary files from Huuhtanen *et al.* [31] and intersected with DEGs identified from Isotype and combination treated mice from **Supplementary Table 1**. (**B**) displays genes upregulated in subsets. (**C**) displays genes downregulated in the subsets. CM = central memory, EM = effector memory.

in FACS buffer (PBS, 2% FBS). Analysis was performed on a BD LSR Fortessa X-20 instrument. The blue form of the Timer protein was detected in the blue (450/40 nm) channel excited off the 405 nm laser. The red form of the Timer protein was detected in the mCherry (610/20 nm) channel excited off the 561 nm laser. A fixable eFluor780-flurescent viability dye (eBioscience) was used for all experiments. Directly conjugated antibodies used in these experiments were CD4 APC or PerCP-Cy5.5 (clone GK1.5, BioLegend), CD4, CD4 Alexa Fluor 700 (clone RM4-4, BioLegend), CD4 BUV737 (clone GK1.5, BD Biosciences), TCR Vβ8.1, 8.2 BUV395 (clone, MR5-2, BD Biosciences) CD4 BUV395 (clone GK1.5, BD Biosciences), CD8a PE-Cy7 (clone 53-6.7, BioLegend), TCRβ FITC (clone H57-597, BioLegend), PD1 PE-Cy7 (clone 29F.1A12, BioLegend), Lag3 APC or PE-Cy7 (clone C9B7W, BioLegend), OX40 APC or PE-Cy7 (clone OX-86, BioLegend), ICOS Alexa Fluor 700 (clone C398.4A, BioLegend), IRF8 PE (clone V3GYWCH, Invitrogen), CD25 PE-Cy7 (clone PC61, BioLegend), CD44 PerCP-Cy5.5. (clone IM7, BioLegend), PD-L1 APC or PE-Cy7 (clone 10F.9G2, BioLegend), IRF4 PE-Cy7 (clone IRF4.3E4, BioLegend), CCR6 APC or PE (clone 29-2L17, BioLegend), CXCR5 APC (clone L138D7, BioLegend), CD19 PE-Cy7 (clone 6D5, BioLegend), CD11b PE-Cy7 (clone M1/70, BioLegend), PD-L1 BV711 (clone 10F.9G2, BioLegend). For intracellular staining of IRF8 or IRF4, the Foxp3 transcription factor staining buffer kit was used according to the manufacturers' instructions (eBioscience). For cell sorting for RNA-seq experiments, single cell suspensions from the spleens of immunized mice were generated and then multiplexed to sort in batches of four on a FACS ARIA FUSION cell sorter (BD Biosciences). Multiplex sorting was performed using the following CD4 antibodies for the four experimental conditions: Isotype (CD4 APC), anti-PD-L1 (CD4 BUV395), anti-Lag3 (BUV737), and combination therapy (CD4 PerCPcy5.5). A dump channel consisting of CD19 PE-Cy7, CD11b PE-CY7 and CD8-Cy7 was used and cells were sorted as live, CD4+CD19-CD11b-CD8-Nr4a3Red+Nr4a3Blue+ (i.e. "responder" CD4+ T cells). For migration assays live, CD4+CD19-CD11b-CD8- were sorted.

In vitro restimulation of adaptively tolerised CD4+ T cells

For the adaptive tolerance model, Tg4 *Nr4a3*-Tocky Tiger (*Il10*-GFP) mice were immunized through subcutaneous injection of 4 mg/kg [4Y] MBP peptide. Twenty-four hours later, mice were euthanised and spleens were removed and digested as described above. Digested cells were washed once and 5 × 10^5 splenocytes cultured for 24 h in 96-well U-bottom plates (Corning) final volume of 200 µl RPMI 1640 containing 10% FCS and penicillin/streptomycin and 55 µM β-mercaptoethanol (Gibco) for the stated time periods in the presence of a range of [4Y]-MBP peptide concentrations. Blocking antibodies (anti-PD-L1 clone MIH5, and anti-Lag3 clone C9B7W) were administered at 20 µg/ml. For functional assessment of the NFAT pathway in promoting OX40 and ICOS expression, Tg4 Nur77-Tempo Tiger (*Il10*-GFP) mice were immunized through subcutaneous injection of 4 mg/kg [4Y] MBP peptide. Twenty-four hours later, mice were euthanised and spleens were removed and digested as described above. Splenocytes were restimulated with 2.5 nM 4Y [MBP] peptide in the presence of a dose range of cyclosporin a (Cambridge Bioscience) and analysed 24 h after *in vitro* culture.

RNA-seq library preparation and analysis

RNA was extracted from lysates using the PureLink RNA Micro Scale Kit (Invitrogen) according to the manufacturer's instructions. 5 ng of RNA was used for generation of sequencing libraries using the Quantseq 3' mRNA-seq Library Preparation kit (Lexogen). Briefly, library generation was commenced with oligodT priming containing the Illumina-specific Read 2 linker sequence. After first strand synthesis, RNA was degraded. Second strand synthesis was initiated by random priming and a DNA polymerase. Random primers contained the illumina-specific Read 1 linker sequence. Double stranded DNA was purified from the reaction using magnetic beads and libraries amplified (18 cycles) and sequences required for cluster generation and sample indexes were introduced. Libraries were normalized and pooled at a concentration of 4 nM for sequencing. Libraries were sequenced using the NextSeq 500 using a High 75 cycle flow cell. Cluster generation and sequencing was then performed and FASTQ files generated. FASTQ files were then processed by Lexogen as follows: Trimming was performed using Cutadapt version 1.18, followed by mapping using STAR version 2.6.1a to the GRCm38 genome. Reads counting as performed using FeatureCounts version 1.6.4. Uniquely mapped read counts conts in the.txt format were used for further analysis using DESeq2 in R version 4.0 [68]. A DESeq dataset was created from a matrix of raw read count data. Data were filtered to remove genes with fewer than 30 reads across all samples. Log2 fold change estimates were generated using the DESeq algorithm and shrinkage using the ashr algorithm [69] to estimate log2 fold changes (lfc). A lfc threshold of 0.2 was set and genes with an adjusted *P* value <.05 and an *s* value <0.005 were used to filter out genes with low expression or negligible gene expression changes. Normalized read counts were transformed using the regularized log (rlog) transformation. Heatmap analysis was performed on the rlog transformed data using the R package gplots. For KEGG pathway analysis clusterProfiler [70], DOSE [71] and biomaRt [72] packages were used. Venn diagrams were generated using the CRAN package VennDiagram. Data are deposited at GEO: GSE260895. Data from Elliot *et al.* [2], which determined the effect of TCR signal strength on Lag3 and PD-1 expression kinetics, is deposited at GEO: GSE165817.

Gene set enrichment analysis (GSEA)

Normalised counts for combination-treated or isotype-treated CD4 T cells from RNA-seq analysis performed in DESeq2 were fed in to GSEA 4.3.3 [73, 74]. 1000 permutations were performed using the gene_set permutation using NFAT and ERK-dependent gene sets as annotated in Wither *et al.* [29]. For the predominantly NFAT-dependent gene set, 283 out of 309 were detected in our dataset. For the predominantly ERK-dependent gene set, 124 out of 136 were detected in our dataset.

TCR signal duration termination by PP2 administration

Nr4a3-Tocky Tg4 Tiger mice were subcutaneously injected with 4 mg/kg [4Y] MBP peptide. Mice were culled 24 h later and spleens were dissociated and single cell suspensions of splenocytes were made using the digest method as described above. Cells were washed once and cultured at 5 × 10^5 cells per well on 96-well U-bottom plates (Corning) in presence of 0.1

μM [4Y]-MBP peptide in a final volume of 200 µl RPMI1640 + L-glutamine (GIBCO) containing 10% FCS and 1% penicillin/streptomycin (Life Technologies). Inhibitors were dissolved in DMSO. PP2 (Sigma, 10 µM) was added at different time points. Cells were incubated at 37°C and 5% CO_2 and analysed at the indicated time points on flow cytometry.

Immunization for Tfh cell responses

C57BL/6J mice were immunized with alum-precipitated (9% aluminium potassium sulfate [Sigma-Aldrich]) NP-OVA conjugate (NP-conjugated ovalbumin), alum NP-OVA. These were respectively prepared by mixing endotoxin-free NP-conjugated ova (kind gift from Prof Kai Toellner, University of Birmingham) with a 9% alum solution. Per mouse a total of 20 µg NP-OVA was mixed with same volume of 9% alum and pH was adjusted using NaOH and HCL. After washing, 20 µg NP-ova/Alum was resuspended in a total volume of 20 µl PBS and injected into the left footpad. 24 h later mice were administrated via the intraperitoneal (i.p.) route with 0.5 mg anti-PD-L1 (clone MIH5), anti-Lag3 (clone C9B7W), combination therapy of their respective isotype control (pooled at 1:1 ratios). On day 8, mice were euthanized and the popliteal lymph node was harvested. LNs were forced through 70 µM filters, before cells were stained for flow cytometric analysis.

Migration assays

To measure migration, FACS purified $CD4^+$ T cells were cultured in a 5-µm polycarbonate 24-well transwell system (Corning). T cells were loaded into the top chamber at a density of 2.5×10^5 cells in 0.1 ml complete media, with the bottom chamber containing either 0 or 100 ng/ml CCL20 (BioLegend) in 0.6 ml complete media. After 4 h, the contents of the bottom chamber were harvested and washed extensively with PBS (+ 2 mM EDTA and 2% FCS), followed by enumeration by flow cytometry. AccuCheck couning beads (Invitrogen) were used to calculate the absolute number of $CD4^+$ T cells in each sample. Migration index was calculated by normalizing cells in the lower chamber compared to the medium alone control from isotype-treated mice.

Analysis of human combination therapy datasets

Differentially expressed genes compared to month 3 or month 1 compared to baseline in CD4 Naïve, CD4 effector memory, and CD4 Treg clusters from human patients on anti-PD-1 and anti-Lag3 therapy were extracted from supplementary files from [31] and intersected with DEGs identified from Isotype and CB mice (**Supplementary Table 1**).

Statistical analysis

For non-RNA-sequencing analysis, statistical analysis was performed on Prism 10 (GraphPad) software. Flow cytometry data were analysed using FlowJo software (BD Biosciences). Statistical analysis for comparison of more than two means was performed using one-way ANOVA with Tukey's multiple comparisons test. For analysis of two factor variable experiments, a two-way repeated-measures ANOVA was performed with Tukey's multiple comparisons tests. For detection of synergy, a two-way ANOVA test was performed factoring in the variables anti-PD-L1 and anti-Lag3 to test for significance of interaction. For non-parametric data a Kruskal–Wallis test was performed with Dunn's multiple comparisons. Variance is reported as mean ± SEM unless stated otherwise; data points represent individual mice. $*P = < .05$, $**P = < .01$, $***P = < .001$, $****P = < .0001$.

Author contributions

Lozan Sheriff (Formal analysis, Investigation, Methodology, Writing - review & editing), Alastair Copland (Formal analysis, Investigation, Methodology, Writing - review & editing), David A.J. Lecky (Investigation, Methodology), Reygn Done (Investigation), Lorna S George (Investigation), Emma Jennings (Investigation), Sophie Rouvray (Investigation), Thomas A.E. Elliot (Investigation), Elizabeth S. Jinks (Investigation), Lalit Pallan (Conceptualization), and David Bending (Conceptualization, Data curation, Formal analysis, Funding acquisition, Methodology, Project administration, Resources, Supervision, Writing - original draft, Writing - review & editing)

Conflict of interest

The authors declare no conflicts of interest.

Ethical approval

All animal experiments were approved by the local animal welfare and ethical review body and authorized under the authority of Home Office licenses P18A892E0A and PP9984349 (held by D.B.).

Data availability

RNA-seq data are deposited at GEO: GSE260895. Nur77-Tempo mice are deposited at the European Mutant Mouse Archive ID EM:15078. All other data are available from the corresponding author (d.a.bending@bham.ac.uk) by request.

Permission to reproduce

Diagrams in the figures and graphical abstract were generated using BioRender.com.

References

1. Smith-Garvin JE, Koretzky GA, Jordan MS. T cell activation. *Annu Rev Immunol* 2009; 27:591–619. https://doi.org/10.1146/annurev.immunol.021908.132706

2. Elliot TAE, Jennings EK, Lecky DAJ et al. Antigen and checkpoint receptor engagement recalibrates T cell receptor signal strength. *Immunity* 2021; 54(11):2481–96.e6. https://doi.org/10.1016/j.immuni.2021.08.020

3. Nishimura H, Nose M, Hiai H et al. Development of lupus-like autoimmune diseases by disruption of the PD-1 gene encoding an ITIM motif-carrying immunoreceptor. *Immunity* 1999; 11(2):141–51. https://doi.org/10.1016/s1074-7613(00)80089-8

4. Krummel MF, Allison JP. CD28 and CTLA-4 have opposing effects on the response of T cells to stimulation. *J Exp Med* 1995; 182(2):459–65. https://doi.org/10.1084/jem.182.2.459

5. Workman CJ, Vignali DA. The CD4-related molecule, LAG-3 (CD223), regulates the expansion of activated T cells. *Eur J Immunol* 2003; 33(4):970–9. https://doi.org/10.1002/eji.200323382

6. Freeman GJ, Long AJ, Iwai Y et al. Engagement of the PD-1 immunoinhibitory receptor by a novel B7 family member leads to negative regulation of lymphocyte activation. *J Exp Med* 2000; 192(7):1027–34. https://doi.org/10.1084/jem.192.7.1027

7. Wolchok JD, Rollin L, Larkin J. Nivolumab and Ipilimumab in Advanced Melanoma. *N Engl J Med* 2017; 377(25):2503–4. https://doi.org/10.1056/NEJMc1714339

8. Tawbi HA, Schadendorf D, Lipson EJ et al; RELATIVITY-047 Investigators. Relatlimab and Nivolumab versus Nivolumab in Untreated Advanced Melanoma. *N Engl J Med* 2022; 386(1):24–34. https://doi.org/10.1056/NEJMoa2109970

9. Okazaki T, Maeda A, Nishimura H et al. PD-1 immunoreceptor inhibits B cell receptor-mediated signaling by recruiting src homology 2-domain-containing tyrosine phosphatase 2 to phosphotyrosine. *Proc Natl Acad Sci U S A* 2001; 98(24):13866–71. https://doi.org/10.1073/pnas.231486598

10. Mizuno R, Sugiura D, Shimizu K et al. PD-1 Primarily Targets TCR Signal in the Inhibition of Functional T Cell Activation. *Front Immunol* 2019; 10:630. https://doi.org/10.3389/fimmu.2019.00630

11. Hui E, Cheung J, Zhu J et al. T cell costimulatory receptor CD28 is a primary target for PD-1-mediated inhibition. *Science* 2017; 355(6332):1428–33. https://doi.org/10.1126/science.aaf1292

12. Linsley PS, Brady W, Urnes M et al. CTLA-4 is a second receptor for the B cell activation antigen B7. *J Exp Med* 1991; 174(3):561–9. https://doi.org/10.1084/jem.174.3.561

13. Freeman GJ, Borriello F, Hodes RJ et al. Murine B7-2, an alternative CTLA4 counter-receptor that costimulates T cell proliferation and interleukin 2 production. *J Exp Med* 1993; 178(6):2185–92. https://doi.org/10.1084/jem.178.6.2185

14. Freeman GJ, Gribben JG, Boussiotis VA et al. Cloning of B7-2: a CTLA-4 counter-receptor that costimulates human T cell proliferation. *Science* 1993; 262(5135):909–11. https://doi.org/10.1126/science.7694363. Jr.

15. Walker LS, Sansom DM. Confusing signals: recent progress in CTLA-4 biology. *Trends Immunol* 2015; 36(2):63–70. https://doi.org/10.1016/j.it.2014.12.001

16. Triebel F, Jitsukawa S, Baixeras E et al. LAG-3, a novel lymphocyte activation gene closely related to CD4. *J Exp Med* 1990; 171(5):1393–405. https://doi.org/10.1084/jem.171.5.1393

17. Baixeras E, Huard B, Miossec C et al. Characterization of the lymphocyte activation gene 3-encoded protein. A new ligand for human leukocyte antigen class II antigens. *J Exp Med* 1992; 176(2):327–37. https://doi.org/10.1084/jem.176.2.327

18. Bawden EG, Wagner T, Schroder J et al. CD4(+) T cell immunity against cutaneous melanoma encompasses multifaceted MHC II-dependent responses. *Sci Immunol* 2024; 9(91):eadi9517. https://doi.org/10.1126/sciimmunol.adi9517

19. Bos R, Sherman LA. CD4+ T-cell help in the tumor milieu is required for recruitment and cytolytic function of CD8+ T lymphocytes. *Cancer Res* 2010; 70(21):8368–77. https://doi.org/10.1158/0008-5472.CAN-10-1322

20. Zhu Z, Cuss SM, Singh V et al. CD4+ T Cell Help Selectively Enhances High-Avidity Tumor Antigen-Specific CD8+ T Cells. *J Immunol* 2015; 195(7):3482–9. https://doi.org/10.4049/jimmunol.1401571

21. Correa K, Dustin ML. Locked and loaded: strong TCR signaling primes anti-PD-1 therapy. *Trends Immunol* 2021; 42(12):1066–8. https://doi.org/10.1016/j.it.2021.10.014

22. Anderton SM, Manickasingham SP, Burkhart C et al. Fine specificity of the myelin-reactive T cell repertoire: implications for TCR antagonism in autoimmunity. *J Immunol* 1998; 161(7):3357–64.

23. Fairchild PJ, Wildgoose R, Atherton E et al. An autoantigenic T cell epitope forms unstable complexes with class II MHC: a novel route for escape from tolerance induction. *Int Immunol* 1993; 5(9):1151–8. https://doi.org/10.1093/intimm/5.9.1151

24. Fugger L, Liang J, Gautam A et al. Quantitative analysis of peptides from myelin basic protein binding to the MHC class II protein, I-Au, which confers susceptibility to experimental allergic encephalomyelitis. *Mol Med* 1996; 2(2):181–8.

25. Maruhashi T, Okazaki IM, Sugiura D et al. LAG-3 inhibits the activation of CD4(+) T cells that recognize stable pMHCII through its conformation-dependent recognition of pMHCII. *Nat Immunol* 2018; 19(12):1415–26. https://doi.org/10.1038/s41590-018-0217-9

26. Maruhashi T, Sugiura D, Okazaki IM et al. Binding of LAG-3 to stable peptide-MHC class II limits T cell function and suppresses autoimmunity and anti-cancer immunity. *Immunity* 2022; 55(5):912–924.e8 e918. https://doi.org/10.1016/j.immuni.2022.03.013

27. Sheriff L, Bending D. Flow cytometric analysis of CD4+ T cell reactivation following anti-PD1 immunotherapy in a transgenic mouse model. *STAR Protoc* 2022; 3(1):101161. https://doi.org/10.1016/j.xpro.2022.101161

28. Jennings E, Elliot TAE, Thawait N et al. Nr4a1 and Nr4a3 reporter mice are differentially sensitive to T cell receptor signal strength and duration. *Cell Rep* 2020; 33(5):108328. https://doi.org/10.1016/j.celrep.2020.108328

29. Wither MJ, White WL, Pendyala S et al. Antigen perception in T cells by long-term Erk and NFAT signaling dynamics. *Proc Natl Acad Sci USA* 2023; 120(52):e2308366120. https://doi.org/10.1073/pnas.2308366120

30. Seth A, Yokokura Y, Choi JY et al. AP-1-independent NFAT signaling maintains follicular T cell function in infection and autoimmunity. *J Exp Med* 2023; 220(5):e20211110. https://doi.org/10.1084/jem.20211110

31. Huuhtanen J, Kasanen H, Peltola K et al. Single-cell characterization of anti-LAG-3 and anti-PD-1 combination treatment in patients with melanoma. *J Clin Invest* 2023; 133(6):e164809. https://doi.org/10.1172/JCI164809

32. Reissig S, Tang Y, Nikolaev A et al. Elevated levels of Bcl-3 inhibits Treg development and function resulting in spontaneous colitis. *Nat Commun* 2017; 8:15069. https://doi.org/10.1038/ncomms15069

33. Yu X, Teng XL, Wang F et al. Metabolic control of regulatory T cell stability and function by TRAF3IP3 at the lysosome. *J Exp Med* 2018; 215(9):2463–76. https://doi.org/10.1084/jem.20180397

34. Cornely R, Pollock AH, Rentero C et al. Annexin A6 regulates interleukin-2-mediated T-cell proliferation. *Immunol Cell Biol* 2016; 94(6):543–53. https://doi.org/10.1038/icb.2016.15

35. Yu H, Leitenberg D, Li B et al. Deficiency of small GTPase Rac2 affects T cell activation. *J Exp Med* 2001; 194(7):915–26. https://doi.org/10.1084/jem.194.7.915

36. Glatigny S, Duhen R, Oukka M et al. Cutting edge: loss of alpha4 integrin expression differentially affects the homing of Th1 and Th17 cells. *J Immunol* 2011; 187(12):6176–9. https://doi.org/10.4049/jimmunol.1102515

37. Boussiotis VA. Molecular and biochemical aspects of the PD-1 checkpoint pathway. *N Engl J Med* 2016; 375(18):1767–78. https://doi.org/10.1056/NEJMra1514296

38. Kouo T, Huang L, Pucsek AB et al. Galectin-3 shapes antitumor immune responses by suppressing CD8+ T cells via LAG-3 and inhibiting expansion of plasmacytoid dendritic cells. *Cancer Immunol Res* 2015; 3(4):412–23. https://doi.org/10.1158/2326-6066.CIR-14-0150

39. Wang J, Sanmamed MF, Datar I et al. Fibrinogen-like protein 1 is a major immune inhibitory ligand of LAG-3. *Cell* 2019; 176(1-2):334–347 e312. https://doi.org/10.1016/j.cell.2018.11.010

40. Guy C, Mitrea DM, Chou PC et al. LAG3 associates with TCR-CD3 complexes and suppresses signaling by driving co-receptor-Lck dissociation. *Nat Immunol* 2022; 23(5):757–67. https://doi.org/10.1038/s41590-022-01176-4

41. Aggarwal V, Workman CJ, Vignali DAA. LAG-3 as the third checkpoint inhibitor. *Nat Immunol* 2023; 24(9):1415–22. https://doi.org/10.1038/s41590-023-01569-z

42. Li N, Wang Y, Forbes K et al. Metalloproteases regulate T-cell proliferation and effector function via LAG-3. *EMBO J* 2007; 26(2):494–504. https://doi.org/10.1038/sj.emboj.7601520

43. Andrews LP, Somasundaram A, Moskovitz JM et al. Resistance to PD1 blockade in the absence of metalloprotease-mediated LAG3 shedding. *Sci Immunol* 2020; 5(49):5. https://doi.org/10.1126/sciimmunol.abc2728

44. Fife BT, Pauken KE, Eagar TN et al. Interactions between PD-1 and PD-L1 promote tolerance by blocking the TCR-induced stop signal. *Nat Immunol* 2009; 10(11):1185–92. https://doi.org/10.1038/ni.1790

45. Schneider H, Downey J, Smith A et al. Reversal of the TCR stop signal by CTLA-4. *Science* 2006; 313(5795):1972–5. https://doi.org/10.1126/science.1131078

46. Woo SR, Turnis ME, Goldberg MV et al. Immune inhibitory molecules LAG-3 and PD-1 synergistically regulate T-cell function to promote tumoral immune escape. *Cancer Res* 2012; 72(4):917–27. https://doi.org/10.1158/0008-5472.CAN-11-1620

47. Andrews LP, Butler SC, Cui J et al. LAG-3 and PD-1 synergize on CD8(+) T cells to drive T cell exhaustion and hinder autocrine IFN-gamma-dependent anti-tumor immunity. *Cell* 2024; 187(16):4355–72.e22. https://doi.org/10.1016/j.cell.2024.07.016

48. Cillo AR, Cardello C, Shan F et al. Blockade of LAG-3 and PD-1 leads to co-expression of cytotoxic and exhaustion gene modules in CD8(+) T cells to promote antitumor immunity. *Cell* 2024; 187(16):4373–88.e15. https://doi.org/10.1016/j.cell.2024.06.036

49. Ngiow SF, Manne S, Huang YJ et al. LAG-3 sustains TOX expression and regulates the CD94/NKG2-Qa-1b axis to govern exhausted CD8 T cell NK receptor expression and cytotoxicity. *Cell* 2024; 187(16):4336–54.e19. https://doi.org/10.1016/j.cell.2024.07.018

50. Speiser DE, Chijioke O, Schaeuble K et al. CD4(+) T cells in cancer. *Nat Cancer* 2023; 4(3):317–29. https://doi.org/10.1038/s43018-023-00521-2

51. Kos K, de Visser KE. The multifaceted role of regulatory T cells in breast cancer. *Annu Rev Cancer Biol* 2021; 5:291–310. https://doi.org/10.1146/annurev-cancerbio-042920-104912

52. Satpathy AT, Granja JM, Yost KE et al. Massively parallel single-cell chromatin landscapes of human immune cell development and intratumoral T cell exhaustion. *Nat Biotechnol* 2019; 37(8):925–36. https://doi.org/10.1038/s41587-019-0206-z

53. Gutierrez-Melo N, Baumjohann D. T follicular helper cells in cancer. *Trends Cancer* 2023; 9(4):309–25. https://doi.org/10.1016/j.trecan.2022.12.007

54. Gu-Trantien C, Loi S, Garaud S et al. CD4(+) follicular helper T cell infiltration predicts breast cancer survival. *J Clin Invest* 2013; 123(7):2873–92. https://doi.org/10.1172/JCI67428

55. Cui C, Wang J, Fagerberg E et al. Neoantigen-driven B cell and CD4 T follicular helper cell collaboration promotes anti-tumor CD8 T cell responses. *Cell* 2021; 184(25):6101–18.e13. https://doi.org/10.1016/j.cell.2021.11.007

56. Shakiba M, Zumbo P, Espinosa-Carrasco G et al. TCR signal strength defines distinct mechanisms of T cell dysfunction and cancer evasion. *J Exp Med* 2022; 219(2):e20201966. https://doi.org/10.1084/jem.20201966

57. Herati RS, Knorr DA, Vella LA et al. PD-1 directed immunotherapy alters Tfh and humoral immune responses to seasonal influenza vaccine. *Nat Immunol* 2022; 23(8):1183–92. https://doi.org/10.1038/s41590-022-01274-3

58. Jing Y, Liu J, Ye Y et al. Multi-omics prediction of immune-related adverse events during checkpoint immunotherapy. *Nat Commun* 2020; 11(1):4946. https://doi.org/10.1038/s41467-020-18742-9

59. Tsukamoto H, Komohara Y, Tomita Y et al. Aging-associated and CD4 T-cell-dependent ectopic CXCL13 activation predisposes to anti-PD-1 therapy-induced adverse events. *Proc Natl Acad Sci USA* 2022; 119(29):e2205378119. https://doi.org/10.1073/pnas.2205378119

60. Tafuri A, Shahinian A, Bladt F et al. ICOS is essential for effective T-helper-cell responses. *Nature* 2001; 409(6816):105–9. https://doi.org/10.1038/35051113

61. Festen EA, Goyette P, Scott R et al. Genetic variants in the region harbouring IL2/IL21 associated with ulcerative colitis. *Gut* 2009; 58(6):799–804. https://doi.org/10.1136/gut.2008.166918

62. Wellcome Trust Case Control C. Genome-wide association study of 14,000 cases of seven common diseases and 3,000 shared controls. *Nature* 2007; 447(7145):661–78. https://doi.org/10.1038/nature05911

63. Chat V, Ferguson R, Simpson D et al. Autoimmune genetic risk variants as germline biomarkers of response to melanoma immune-checkpoint inhibition. *Cancer Immunol Immunother* 2019; 68(6):897–905. https://doi.org/10.1007/s00262-019-02318-8

64. Bending D, Prieto Martin P, Paduraru A et al. A timer for analyzing temporally dynamic changes in transcription during differentiation in vivo. *J Cell Biol* 2018; 217(8):2931–50. https://doi.org/10.1083/jcb.201711048

65. Burton BR, Britton GJ, Fang H et al. Sequential transcriptional changes dictate safe and effective antigen-specific immunotherapy. *Nat Commun* 2014; 5:4741. https://doi.org/10.1038/ncomms5741

66. Elliot TAE, Jennings EK, Lecky DAJ et al. Nur77-Tempo mice reveal T cell steady state antigen recognition. *Discov. Immunol.* 2022; 1(1):kyac009. https://doi.org/10.1093/discim/kyac009

67. Tsushima F, Iwai H, Otsuki N et al. Preferential contribution of B7-H1 to programmed death-1-mediated regulation of hapten-specific allergic inflammatory responses. *Eur J Immunol* 2003; 33(10):2773–82. https://doi.org/10.1002/eji.200324084

68. Love MI, Huber W, Anders S. Moderated estimation of fold change and dispersion for RNA-seq data with DESeq2. *Genome Biol* 2014; 15(12):550. https://doi.org/10.1186/s13059-014-0550-8

69. Stephens M. False discovery rates: a new deal. *Biostatistics* 2017; 18(2):275–94. https://doi.org/10.1093/biostatistics/kxw041

70. Yu G, Wang LG, Han Y et al. clusterProfiler: an R package for comparing biological themes among gene clusters. *OMICS* 2012; 16(5):284–7. https://doi.org/10.1089/omi.2011.0118

71. Yu G, Wang LG, Yan GR et al. DOSE: an R/Bioconductor package for disease ontology semantic and enrichment analysis. *Bioinformatics* 2015; 31(4):608–9. https://doi.org/10.1093/bioinformatics/btu684

72. Durinck S, Spellman PT, Birney E et al. Mapping identifiers for the integration of genomic datasets with the R/Bioconductor package biomaRt. *Nat Protoc* 2009; 4(8):1184–91. https://doi.org/10.1038/nprot.2009.97

73. Subramanian A, Tamayo P, Mootha VK et al. Gene set enrichment analysis: a knowledge-based approach for interpreting genome-wide expression profiles. *Proc Natl Acad Sci USA* 2005; 102(43):15545–50. https://doi.org/10.1073/pnas.0506580102

74. Mootha VK, Lindgren CM, Eriksson KF et al. PGC-1alpha-responsive genes involved in oxidative phosphorylation are coordinately downregulated in human diabetes. *Nat Genet* 2003; 34(3):267–73. https://doi.org/10.1038/ng1180